

Amortized Spectral Kernel Discovery via Prior-Data Fitted Network

Kaustubh Sharma ^{*1} Srijan Tiwari ^{*1} Ojasva Nema ^{*2} Parikshit Pareek ¹

Abstract

Prior-Data Fitted Networks (PFNs) enable efficient amortized inference but lack transparent access to their learned priors and kernels. This opacity hinders their use in downstream tasks, such as surrogate-based optimization, that require explicit covariance models. We introduce an interpretability-driven framework for *amortized spectral discovery* from pre-trained PFNs with decoupled attention. We perform a mechanistic analysis on a trained PFN that identifies attention latent output as the key intermediary, linking observed function data to spectral structure. Building on this insight, we propose decoder architectures that map PFN latents to explicit spectral density estimates and corresponding stationary kernels via Bochner’s theorem. We study this pipeline in both single-realization and multi-realization regimes, contextualizing theoretical limits on spectral identifiability and proving consistency when multiple function samples are available. Empirically, the proposed decoders recover complex multi-peak spectral mixtures and produce explicit kernels that support Gaussian process regression with accuracy comparable to PFNs and optimization-based baselines, while requiring only a single forward pass. This yields orders-of-magnitude reductions in inference time compared to optimization-based baselines.

1. Introduction

The central question in modern probabilistic modeling is the tradeoff between *structural inductive bias* and *computational scalability*. Kernel-based methods, particularly Gaus-

^{*}Equal contribution ¹Department of Electrical Engineering, Indian Institute of Technology Roorkee (IIT Roorkee), India

²Department of Material Science & Engineering, Indian Institute of Technology Roorkee (IIT Roorkee), India. Correspondence to: Parikshit Pareek <pareek@ee.iitr.ac.in>, This work was supported by the ANRF PM Early Career Research Grant (ANRF/ECRG/2024/001962/ENS), the IIT Roorkee Faculty Initiation Grant (IITR/SRIC/1431/FIG-101078). <>.

sian Processes (GPs), offer exact uncertainty quantification and, through the covariance kernel, an explicit language to describe properties like periodicity, smoothness, and stationarity (Rasmussen & Williams, 2006). This explicit structure is indispensable in scientific discovery, where the goal is often to identify the data-generating mechanism (e.g., the spectral density of a signal) rather than merely fitting points. However, beyond the use of standard kernels (Rasmussen & Williams, 2006), identifying the correct kernel structure is computationally prohibitive. Methods such as Deep Kernel Learning (DKL) (Wilson et al., 2015) or the Automatic Statistician (Lloyd et al., 2014) rely on expensive iterative marginal likelihood optimization for every new dataset, creating a bottleneck that prevents real-time deployment.

Conversely, amortized Bayesian inference methods, including Prior-Data Fitted Networks (PFNs) (Müller et al., 2024) and Neural Processes (Garnelo et al., 2018), address the scalability challenge. By pre-training on a distribution of priors, PFNs learn to map datasets directly to posterior predictive distributions in a single forward pass. These models achieve strong predictive performance and can approximate Bayesian inference procedures across a wide range of tasks (Müller et al., 2025; Müller et al., 2024; Nagler, 2023; Adriænsen et al., 2023). However, this amortization comes at the cost of **structural opacity**. The spectral density and covariance structure that define the Bayesian prior are no longer explicitly represented, but instead are implicitly encoded in the network parameters, limiting interpretability and downstream structured reasoning (Müller et al., 2025).

This work bridges this gap by proposing a framework for *amortized spectral and kernel discovery*. We address two limitations emphasized in recent foundational perspectives on PFNs (Müller et al., 2025): (1) the lack of mechanistic transparency and (2) the absence of explicit, portable representations of the latent structure learned during amortized inference. We show that PFNs do not merely memorize predictions; rather, they construct structured internal representations that encode properties of the data-generating process. We introduce a decoding framework that extracts this implicit information in the form of an explicit spectral density, from which a stationary covariance kernel is obtained via Bochner’s theorem.

Our approach reframes the PFN from a black-box predictor

into a **zero-shot spectral inference engine**. Instead of performing iterative kernel optimization at test time like DKL, the model processes a context dataset and directly outputs an explicit spectral representation in a single forward pass. This spectral representation is then deterministically converted into a stationary kernel via Bochner’s theorem. We study this process in two complementary regimes: *single-function identification*, where only one realization of a function is available and only partial spectral information is statistically identifiable, and *multi-function identification*, where multiple realizations from a shared generative process permit full recovery of the spectral density.

Positioning and Contributions: We advance recent progress on PFNs (Müller et al., 2025) by asking a mechanistic question: *if a PFN approximates GP inference, where and how is spectral information represented?* Focusing on PFNs trained with Decoupled-Value Attention (DVA) (Sharma et al., 2025), we show that the attention mechanism induces a separation between spatial similarity and signal amplitude. This architectural property yields an identifiable *spectral manifold* within the latent representation. Conceptually, this induces a simple inference pipeline having contextual data set $\mathcal{D}_{\text{ctx}} = \{X_{\text{ctx}}, Y_{\text{ctx}}\}$

$$\mathcal{D}_{\text{ctx}} \xrightarrow[\text{Attention}]{\text{DVA}} H \& V \xrightarrow[\text{Decoders}]{\text{Proposed}} S(\omega) \xrightarrow[\text{Theorem}]{\text{Bochner}} k(\tau)$$

where, value encodings is given as V , the PFN maps data to a latent representation H which encodes an implicit estimate of the spectral density $S(\omega)$, and the stationary kernel $k(\tau)$ follows directly from this spectrum. Building on this observation, we develop an amortized spectral decoding framework that makes this pipeline explicit, yielding stationary surrogate kernels without iterative test-time optimization. Our main contributions are:

- **Mechanistic evidence of spectral encoding:** Through probing and ablation analyses, we show that DVA-PFN attention representations (H) contains the spectral content of the input function, indicating that PFNs implicitly perform spectral estimation as part of inference.
- **Amortized spectral decoding across regimes:** We propose a decoder that extracts explicit spectral densities from *frozen PFNs*¹ in both single-function and multi-function realization settings, accounting for the distinct statistical identifiability properties of each regime.
- **Fundamental limits of spectral recovery:** We characterize what aspects of the spectral density are identifiable from data. We show that spectral weights are non-identifiable from a single normalized realization, but become identifiable with multiple independent realizations, and we derive an unbiased estimator to recover the missing global scale.

¹Pre-trained PFN with no weights update during inference.

- **Empirical comparison with iterative baselines:** We show that kernels constructed from decoded spectral representations via Bochner’s theorem achieve GP regression performance comparable to PFNs, Deep Kernel Learning and Random Fourier Feature methods, while avoiding iterative test-time optimization and enabling substantial inference speedups.

Scope of the decoded kernel: Firstly, we are not claiming that PFNs are the only way to predict kernels. Our idea is to show that PFNs, which are becoming foundational tools for AutoML, already contain this information. Thus, the value of our method is Interpretability and Reuse, not just raw performance. Further, the kernels recovered in this work are explicit stationary surrogate kernels obtained by applying Bochner’s theorem to decoded spectral densities. They are not exact reconstructions of the PFN’s internal attention mechanism nor guaranteed to match the true data-generating GP kernel. Rather, they capture the dominant second-order statistics encoded in the PFN representation. We evaluate kernel quality by using the decoded kernels as plug-in covariances for GP regression, treating predictive performance as a proxy for the fidelity of the recovered spectral structure.

2. Background and Related Works

2.1. Prior-Data Fitted Networks with DVA

Prior-Data Fitted Networks (PFNs) (Müller et al., 2024) enable amortized Bayesian inference by training a neural set-predictor on a vast distribution of synthetic datasets. Formally, given a prior $p(\mathcal{D})$ over supervised learning tasks, we sample datasets $\mathcal{D}_k = \{(x_i, y_i)\}_{i=1}^N \sim p(\mathcal{D})$. Each dataset is partitioned into a context set $\mathcal{D}_{\text{ctx}} = (X_{\text{ctx}}, Y_{\text{ctx}})$ containing observed pairs, and a query set $\mathcal{D}_{\text{q}} = (X_{\text{q}}, Y_{\text{q}})$ containing targets to predict. The model parameters θ are optimized to minimize the expected Negative Log-Likelihood (NLL):

$$\mathcal{L}(\theta) = \mathbb{E}_{\mathcal{D} \sim p(\mathcal{D})} \left[- \sum_{(x, y) \in \mathcal{D}_{\text{q}}} \log q_{\theta}(y | x, \mathcal{D}_{\text{ctx}}) \right]. \quad (1)$$

To improve scaling and localization in high-dimensional physical systems, we employ the Decoupled-Value Attention (DVA) mechanism proposed by Sharma et al. (2025). Unlike standard Transformers which attend over joint input-output embeddings, DVA structurally separates the roles of inputs and outputs to mirror the GP update rule.

As defined in Sharma et al. (2025), attention affinities are derived exclusively from the input features, while the values are derived solely from the targets. Let ϕ_x and ϕ_y be the input and output encoders, and W_q, W_k, W_v be learnable linear projections. We compute the query matrix Q from

the query points X_q , and the key K and value V matrices from the context data $X_{\text{ctx}}, Y_{\text{ctx}}$ as follows:

$$Q = W_q \phi_x(X_q), K = W_k \phi_x(X_{\text{ctx}}), V = W_v \phi_y(Y_{\text{ctx}})$$

We use standard MLP as $\phi_y(\cdot)$ and Fourier Feature Encoder as $\phi_x(\cdot)$. The latent representation H is then synthesized via dot-product attention:

$$H = \text{Softmax} \left(QK^\top / \sqrt{d_k} \right) V. \quad (2)$$

This formulation ensures that the attention weights depend purely on spatial similarity in the input domain, while V propagates the signal amplitude information. In this work, we leverage this structural decoupling to mechanistically interpret H as a spectral manifold, where the spatial attention weights act as a tunable filter bank over the input frequencies.

2.2. Kernel and Prior Learning

GPs provide a flexible nonparametric framework for modeling unknown functions, where prior assumptions about smoothness and structure are encoded through a covariance kernel $k(x, x')$ (Rasmussen & Williams, 2006). For stationary processes, the kernel admits an equivalent description in the frequency domain. By Bochner's theorem, any continuous shift-invariant kernel is uniquely characterized by a non-negative spectral density, and the kernel is obtained as its Fourier transform (Stein, 1999). This makes the spectral density a natural object for describing periodicity, smoothness, and long-range structure. It also motivates expressive *Spectral Mixture* constructions, which model $S(\omega)$ as a mixture of Gaussians and thereby capture complex patterns that standard kernels (e.g., Radial Basis) fail to represent.

To improve the scalability of kernel methods, **Random Fourier Features (RFF)** approximate stationary kernels by sampling frequencies from a chosen spectral density and mapping inputs into a randomized feature space (Rahimi & Recht, 2007). While this enables efficient linear inference, performance depends strongly on the prescribed spectral density, which is typically fixed and not adapted to the data. The **Deep Kernel Learning (DKL)** addresses this by learning data-dependent representations through a neural network transformation applied before a base kernel (Wilson et al., 2015). Although this allows the effective kernel to adapt to the data, DKL requires per-dataset optimization of the marginal likelihood and can be sensitive to overfitting in the learned representation (Ober et al., 2021). Parallelly, the **Automatic Statistician** (Duvenaud et al., 2013; Lloyd et al., 2014) formulates kernel learning as a combinatorial search over compositions of base kernels. This approach enables automatic discovery and interpretation of high-level structure. Despite their expressivity, both compositional

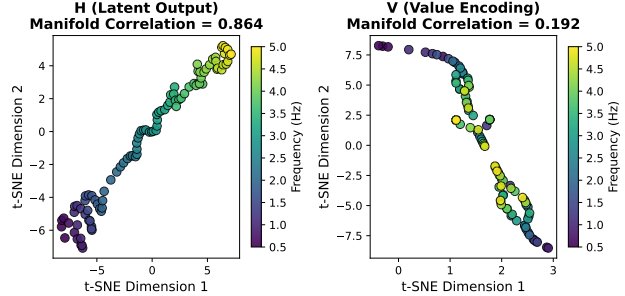


Figure 1. t-SNE visualization of PFN embeddings. H (left) forms a smooth manifold ordered by frequency, while V (right) shows weaker spectral structure.

kernel search and DKL are slow as they rely on iterative, dataset-specific optimization procedures.

A key limitation of existing kernel learning methods is that kernel or spectral parameters are inferred separately for each dataset via *task-specific* training or optimization. They do not amortize spectral discovery as done for Bayesian Inference by PFNs.

Beyond kernel methods, several amortized inference frameworks avoid test-time optimization by mapping context sets directly to predictions, including Conditional Neural Processes and Transformer-based variants (Garnelo et al., 2018; Jenson et al., 2025; Chang et al., 2025). Related work on implicit neural representations and Fourier-based embeddings shows that neural networks can efficiently capture high-frequency structure (Sitzmann et al., 2020; Tancik et al., 2020). However, these approaches are primarily optimized for prediction: the covariance structure governing the model's behavior remains implicit and entangled in the learned representations. They do not decode an explicit spectral density and corresponding stationary kernel.

3. Mechanistic Analysis of PFNs

To address the interpretability limitations of PFNs (Müller et al., 2025), we conduct a systematic mechanistic analysis of pre-trained PFNs. Our goal is to identify **where** information about the data-generating spectral density is encoded within the architecture, and **how** this information can be accessed to enable explicit spectral and kernel construction.

We analyze the primary computational stages of the PFN, including the query and key encodings, the value encoding, and the latent representation H from (2). Our central hypothesis is that *representations like V and H encode the spectral information of the context dataset*. This implies that an implicit estimate of the spectral density $S(\omega)$ is present in H or V . Our investigation reveals following key findings:

Key Result 1: [Spectral Manifold Structure] We visualize learned representations for sinusoidal signals in $[0.5, 5.0]$ Hz using t-distributed Stochastic Neighbor Embedding (t-SNE)

in Figure 1. It shows that the latent attention output H forms a smooth two-dimensional space strongly correlated with frequency (Pearson $\rho = 0.86$), whereas value encodings V exhibit substantially weaker structure ($\rho = 0.19$). This separation is a direct consequence of the mechanical role of DVA. As formalized by Tsai et al. (2019), the attention operation with input only query and key is mathematically equivalent to *Nadaraya–Watson kernel regression* (Nadaraya, 1964), where the softmax induces data-dependent similarity weighting. Crucially, the query–key dot products approximate a shift-invariant weighting $\approx K(x_i - x_j)$ in PFNs trained with DVA². Under this condition, the attention mechanism performs a form of *discrete convolution* (Cordonnier et al., 2020), integrate local observations across the input domain. While the value embeddings V are dominated by point-wise amplitude information, not the global signal information. By the convolution theorem, such filtering concentrates periodic structure into a global representation H that correlates strongly with the underlying spectral density $S(\omega)$.

Key Result 2: [Latent Rectification and Necessity of Attention Pooling] Building on Key Result 1, which establishes that H encodes global spectral structure, we quantify how different components of the spectral density $S(\omega)$ are accessible from H . Using linear probes (Table 3 in Appendix B), we find that H supports near-perfect recovery of dominant frequencies ($R^2 = 0.998$) even under simple mean pooling. Mathematically, this indicates that PFNs perform *non-linear rectification* within their MLP layers because if H were a linear superposition of oscillatory components, mean pooling would result in cancellation ($\int \sin(\omega t) dt \approx 0$). Instead, H encodes a rectified representation proportional to the *spectral power* of the signal, making frequency information linearly accessible.

However, this accessibility is limited in the presence of multiple oscillatory components. While the locations of spectral peaks (frequencies) remain accurately recoverable ($R^2 = 0.96$ in Table 4), estimation of their relative amplitudes—corresponding to spectral weights in $S(\omega)$ degrades substantially under mean pooling ($R^2 \approx 0.14$). This is because uniform aggregation collapses spatial variation in H into a single summary statistic, obscuring how spectral energy is distributed across components. Consequently, distinct amplitude configurations can induce similar pooled representations, leading to ambiguity in weight estimation.

To address this, we use **Multi-Query Attention Pooling** (Lee et al., 2019), which extracts multiple learned summaries from H at different offsets. This provides complementary views of the latent spectral structure, enabling the

²In DVA, $q(x) = W_Q \phi(x)$ and $k(x) = W_K \phi(x)$ for an arbitrary encoding ϕ . Thus $q(x_i)^\top k(x_j) = \phi(x_i)^\top W_Q^\top W_K \phi(x_j) = \kappa(x_i - x_j)$ for any translation-covariant ϕ , yielding shift-invariant attention weights after softmax normalization.

proposed decoder to disentangle contributions from overlapping components that are otherwise conflated by mean pooling. Consistent with this interpretation, attention pooling yields no improvement in single-component settings (0.0% difference), but produces increasing gains as spectral complexity grows (+3.8% on hard and +5.8% on very hard tasks) as shown in Figure 9 in Appendix B.

These findings directly motivates the decoding pipeline presented in Section 5, in which H serves as the key latent object linking observed data to explicit spectral and kernel representations. Full experimental protocols to test the proposed hypothesis are provided in Appendix A.

4. Statistical Identifiability of Spectral Density

Before describing the decoder architectures, we must rigorously characterize what information regarding the spectral density prior and kernel is fundamentally retrievable from the data. We contextualize the information-theoretic limits of spectral density mapping from functional data to PFN latent space based spectral kernel decoding in two regimes: *single-realization setting* and *multi-realization setting*.

4.1. The Single-Realization Limit

In the single-realization setting, the model observes a single realization (context set) sampled from unknown spectral density. A critical question is *whether this single function realization is sufficient to fully reconstruct the underlying spectral density and kernel from it*. The following theorem establishes a fundamental bound on this capability.

Theorem 4.1 (Single-function non-identifiability of spectral weights). *Let $f : \mathbb{R} \rightarrow \mathbb{R}$ be a zero-mean stationary Gaussian process $f \sim \mathcal{GP}(0, k)$, where $k(\tau)$ is a continuous stationary kernel with spectral density constructed using $w_q > 0$ as $S(\omega) = \sum_{q=1}^Q w_q \mathcal{N}(\omega | \mu_q, \sigma_q^2)$.*

If $\{f(x_i)\}_{i=1}^N$ be a single realization observed on a fixed grid $\{x_i\}_{i=1}^N \subset \mathbb{R}$, and suppose the observations are normalized to unit empirical variance. Then the spectral weights $\{w_q\}_{q=1}^Q$ are not identifiable from this single realization, except up to a common multiplicative constant, even in the limit $N \rightarrow \infty$.

Proof of the Theorem 4.1 is given in Appendix E.1. The theorem above implies that a neural network trying to regress absolute kernel variance from normalized data is an ill-posed problem. The relative spectral power (shape) is recoverable, but the global scale is statistically ambiguous. To resolve this without forcing the network to “hallucinate” a scale, we decouple the magnitude estimation. We employ the following analytical estimator to recover the missing degree of freedom in terms of single scale:

Proposition 4.2 (Unbiased estimation of the kernel scale).

Let $\mathbf{f} = (f(x_1), \dots, f(x_N))^\top$ be a single realization of $f \sim \mathcal{GP}(0, \alpha K)$, where K is a fixed positive semi-definite matrix encoding the decoded kernel shape and $\alpha > 0$ is an unknown multiplicative constant. Then $\|\mathbf{f}\|_2^2 / \text{tr}(K)$ is an unbiased estimator of the multiplicative constant α .

The proof is given in Appendix E.2. This proposition provides the theoretical justification for the **Analytical Scaling** module which will be used in decoders (Figure 2). By analytically computing α post-hoc, we allow the decoder to focus exclusively on the learnable aspects of the spectral density (frequency and bandwidth), ensuring the final covariance is both spectrally accurate and energetically consistent.

4.2. The Multi-Realization Guarantee

In the multi-realization setting, the PFN observes multiple independent functions sampled from the same underlying physical process (spectral density). Here, we show that the ambiguity vanishes, providing a consistency guarantee for proposed decoder.

Theorem 4.3 (Identifiability of spectral weights from multiple realizations). *Let $\{f_m\}_{m=1}^M$ be independent realizations drawn from a zero-mean stationary GP with kernel $k(\tau)$ and spectral density $S(\omega) = \sum_{q=1}^Q w_q \mathcal{N}(\omega | \mu_q, \sigma_q^2)$ with $w_q > 0$. Assume each realization is observed on a common fixed input grid $\{x_i\}_{i=1}^N \subset \mathbb{R}$. Then, as the number of realizations M increases, the spectral weights $\{w_q\}_{q=1}^Q$ become identifiable from the empirical second-order statistics of the observed functions.*

Proof of Theorem 4.3 is given in Section E.3. This theorem guarantees that the spectral density decoder task is well-posed when multiple context functions are available. As the PFN is pre-trained on a distribution of tasks (effectively seeing large M during training), it implicitly learns to aggregate second-order statistics. Theorem 4.3 confirms that our method converges to the true data-generating prior as the number of context functions increases, validating the extraction of explicit spectral density priors from implicit attention mechanisms.

While Theorem 4.3 guarantees that spectral weights are statistically recoverable, the computational cost of performing this estimation classically is significant. Using M realizations to empirically estimate the kernel matrix (following the proof outlined in Appendix E.3) entails a runtime complexity of $\mathcal{O}(MN^2)$. Extending this to large-scale settings with high-frequency data becomes prohibitive very quickly. This computational bottleneck is precisely what our framework addresses: by amortizing the cost of spectral integration during pre-training, we replace the expensive $\mathcal{O}(MN^2)$ estimation with a rapid forward pass, achieving the theoretical limit of identifiability without the runtime penalty.

5. Proposed Filter Bank Decoder

The mechanistic analysis in Section 3 shows that PFNs encode spectral information as a smooth manifold within the latent attention representation, and signal amplitude information is in value embeddings. To bridge the gap between the implicit latent state information and the explicit mathematical objects, spectral densities and derived kernels, we propose a **Filter Bank Decoder** architecture in Figure 2.

This decoder maps frozen PFN representations to an explicit *parametric spectral density*, which is subsequently converted into a stationary kernel via Bochner’s theorem. The architecture operates via two decoders, mirroring the two statistical regimes identified in Section 4:

1. **Multi-Realization Decoder:** Infers a full spectral mixture (frequencies, bandwidths, and weights) from multiple independent realizations, leveraging the identifiability guarantee of Theorem 4.3.
2. **Single-Realization Decoder:** Infers dominant frequencies and bandwidths from a single realization, with global scale recovered analytically using Proposition 4.2 to resolve the ambiguity identified in Theorem 4.1.

Architecture and Latent Pooling: The decoder takes as input a context set \mathcal{D}_{ctx} — either a single function $\mathbf{f} \sim S(\omega^*)$ or multiple iid function samples $\{\mathbf{f}_m\}_{m=1}^M \sim S(\omega^*)$. These inputs are then processed through the *frozen* PFN to extract:

- **Attention Output (H):** Following Figure 6 related discussion, we use H to recover the spectral support i.e. locations of peaks.
- **Value Encoding (V):** We use value encoding V , which contains the raw signal values, to obtain scaling information suppressed in H due to softmax normalization.

To aggregate these spatially distributed features, we employ independent Multi-Query Attention (MQA) pooling modules following the **Key Result 2** in Section 3:

$$\mathbf{z}_H = \text{MQA}_H(H), \quad \mathbf{z}_V = \text{MQA}_V(V). \quad (3)$$

This allows the decoder to learn specific “read” operations to extract spectral peaks without washing out high-frequency information. These pooled summaries are concatenated and fused via a multi-layer perceptron (MLP) Φ , yielding a global context vector $\mathbf{z} = \Phi([\mathbf{z}_H \parallel \mathbf{z}_V])$ which serves as the input for spectral parameter prediction.

Spectral Parameter Prediction: We adopt a *filter bank* formulation to naturally handle the sparsity of spectral mixture kernels. We discretize the frequency domain $[\mu_{\min}, \mu_{\max}]$ into B bins of width $\Delta = (\mu_{\max} - \mu_{\min})/B$. The global context \mathbf{z} is fed into three parallel prediction heads:

1. **Bin Classifier:** Predicts a probability $p_b \in [0, 1]$ for each bin b , indicating the presence of a spectral peak.
2. **Offset-Bandwidth Regressor:** Predicts a tuple (δ_b, σ_b)

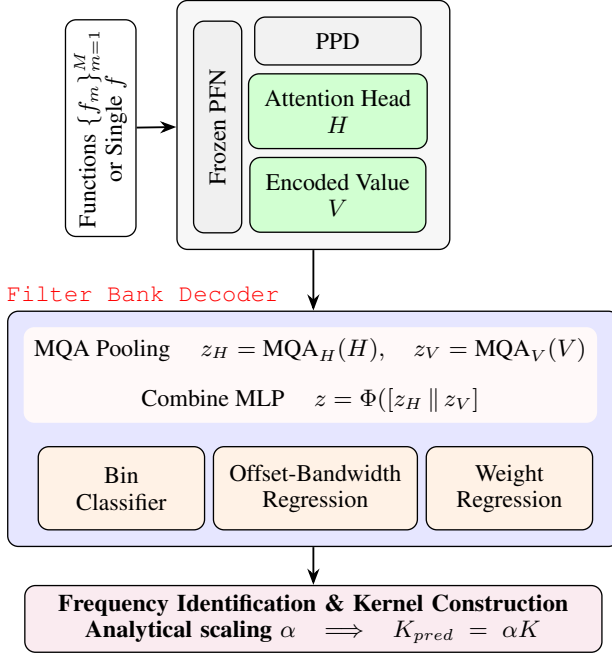


Figure 2. Architectural overview of the proposed Filter Bank Decoder: The framework operates on either single or multiple function realizations processed by a frozen PFN. Latent representations (H, V) are aggregated via Multi-Query Attention (MQA) pooling. A multi-head decoder identifies active spectral bins and regresses precise filter parameters. Finally, the explicit stationary kernel is reconstructed via Bochner’s theorem, utilizing the analytical scaling factor α to ensure energy consistency with the observations.

for each bin. Here, $\delta_b \in [0, 1]$ is a relative offset refining the center frequency $\mu_b = \mu_{\min} + (b + \delta_b)\Delta$, and $\sigma_b > 0$ represents the spectral bandwidth (inverse lengthscale).

3. Weight Regressor (Multi-Realization Only): Predicts the relative spectral power $w_b \geq 0$ for active bins.

In single-realization settings, Theorem 4.1 states that relative spectral weights are non-identifiable. Consequently, we disable the Weight Regressor and assign uniform weights $w_b = 1$ to all active bins, relying on the analytical scaling (described below) to fit the signal envelope.

Kernel Reconstruction via Bochner’s Theorem: These predicted parameters define a sparse spectral density mixture. By applying the inverse Fourier transform (Bochner’s Theorem), we construct the stationary surrogate kernel:

$$K(\tau) = \sum_{b=1}^B \mathbb{I}[p_b > \gamma] w_b \exp(-2\pi^2 \sigma_b^2 \tau^2) \cos(2\pi \mu_b \tau).$$

Here, γ is a classification threshold and $\mathbb{I}[\cdot]$ is indicator function. Finally, to ensure the kernel magnitude matches the observed signal energy and to resolve the scale ambiguity proved in Theorem 4.1, we apply the *global analytical scaling* derived in Proposition 4.2 as $\alpha = \|\mathbf{f}\|_2^2 / \text{tr}(K)$, to obtain

final predicted kernel as $K_{\text{pred}} = \alpha K$. This hybrid approach, learning the spectral shape via a neural network while solving for the scale analytically, ensures the decoded kernel is both structurally accurate and energetically consistent.

Training Mechanism for Decoders: The decoders are trained to minimize a composite loss comprising binary cross-entropy (BCE) for peak detection and masked Mean Squared Error (MSE) for parameter regression:

$$\mathcal{L} = \mathcal{L}_{\text{BCE}}(\mathbf{p}, \mathbf{y}_{\text{bin}}) + \lambda \sum_{b \in \text{active}} \|\boldsymbol{\theta}_b - \boldsymbol{\theta}_b^*\|^2, \quad (4)$$

where $\mathbf{y}_{\text{bin}} \in \{0, 1\}^B$ is the ground-truth bin activation, $\boldsymbol{\theta}_b = (\delta_b, \sigma_b, w_b)$ are the predicted parameters, and $\boldsymbol{\theta}_b^*$ are the ground-truth spectral parameters. The regression loss is masked to only penalize bins containing true spectral peaks. To stabilize training, we employ a *Curriculum Learning* strategy. The decoder is first trained on signals with simple single-component spectra ($n_p = 1$), then two-component spectra ($n_p = 2$), and finally the full mixture distribution $n_p \in \{1, \dots, 4\}$. This ensures the model learns to localize dominant frequencies before attempting to resolve complex spectral interactions. More details about decoder training is given in Appendix C.

6. Experimental Results and Discussions

We evaluate our framework on multiple synthetic spectral mixture datasets. Our experiments are designed to answer the following questions, aligned with the proposed inference pipeline $\mathcal{D}_{\text{ctx}} \rightarrow H \rightarrow S(\omega) \rightarrow k(\tau)$: **(1)** Can the *Multi-Realization Decoder* recover the underlying spectral density from multiple function realizations? **(2)** How do the resulting amortized kernels, in both single- and multi-realization settings, compare to standard kernels and iterative baselines such as DKL and RFF in terms of predictive accuracy and inference efficiency? We further evaluate the performance of the proposed decoders on five- and ten-dimensional datasets.

6.1. Multi-Realization Setting

We evaluate our method on synthetic data generated from stationary GP with spectral mixture densities. Each spectral density consists of 1 to 4 Gaussian components randomly, with center frequencies sampled uniformly from $\mu \sim U[0.5, 3.0]$ Hz and bandwidths from $\sigma \sim U[0.01, 0.05]$. For each configuration, functions are sampled on a fixed input grid and normalized following the pre-trained PFN preprocessing protocol. This setup allows us to systematically control spectral complexity while directly evaluating recovery of the underlying spectral density and its induced kernel.

Figure 3 shows the Wasserstein distance between the true and decoded spectral densities as a function of the number of observed one-dimensional function realizations M .

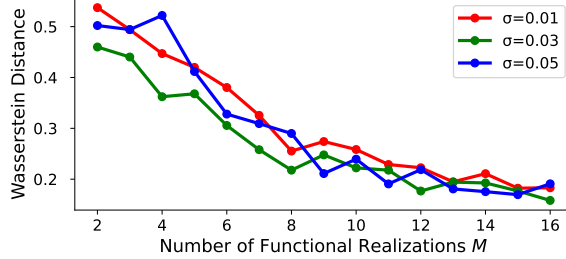


Figure 3. Wasserstein distance between true and predicted spectral densities as a function of the number of GP samples. Similar trends across different bandwidths σ reflect the trade-off between peak sharpness and frequency localization under the Wasserstein metric.

Across all bandwidths, the distance decreases monotonically with the number of realizations, consistent with the identifiability guarantee of Theorem 4.3. Curves corresponding to different bandwidths σ exhibit similar trends. This behavior arises from properties of the Wasserstein metric itself: *narrow spectra (small σ) incur high transport cost for small frequency misalignments, while broader spectra (large σ) are more tolerant to frequency error but harder to localize precisely*. These opposing effects result in comparable Wasserstein distances across bandwidths. Further, Figure 4 provides qualitative confirmation of the proposed decoder’s ability to approximate spectral density mixtures. The decoded spectral densities closely match the ground truth across increasing levels of complexity. Notably, the decoder correctly identifies peak locations even in the presence of overlapping components, indicating that the PFN latent representation preserves fine-grained frequency information sufficient for amortized spectral estimation. Figure 12 in Appendix D shows the kernel matrices³ K_{pred} for increasing spectral complexity.

The comparative performance of K_{pred} , constructed from decoded spectral densities, against an oracle GP shows that decoded kernels provide MSE in same order of magnitude, even when functions belong to spectral density having four components (Table 6). For more results on out-of-distribution kernel families see Appendix D. Across periodic and spectral mixture kernels, the multi-realization decoder matches or at par with oracle GP without any iterative optimization. This indicates that PFNs implicitly encode reusable spectral priors that can be extracted amortized and translated into effective kernels via Bochner’s theorem.

6.2. Single-Realization Setting

Considering the limitations of spectral recovery with single realization established in Theorem 4.1, the goal in this regime is to test the quality of the *surrogate stationary kernel* when used in GP for inference. To do this we perform a

³Decoded spectral densities are converted deterministically into stationary kernels via Bochner’s theorem.

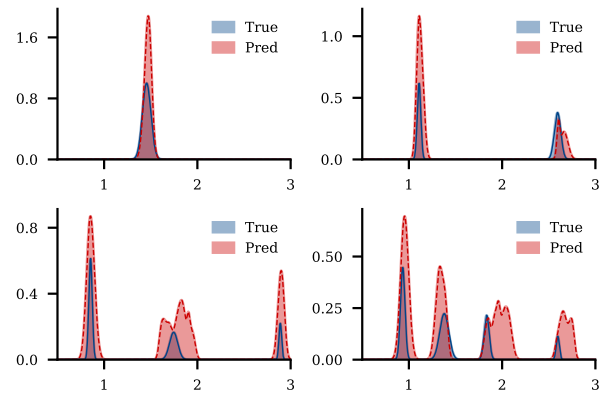


Figure 4. Spectral density recovery. The horizontal axis represents frequency ω (Hz) and the vertical axis represents the spectral density magnitude $S(\omega)$. Blue solid curves denote the ground truth density, while red dashed curves indicate the explicit density recovered by Multi realization decoder. The model accurately identifies peak locations and bandwidths across varying mixture complexities (1–4 components).

kernel cookbook experiment.

This experiment comprising data generated from multiple standard kernel families (including RBF, Periodic, and their compositions). Given a single one-dimensional context function, the decoder’s task is to predict a spectral representation, construct a stationary kernel via Bochner’s theorem, and apply analytical scaling. We then assess whether the resulting K_{pred} supports GP regression performance comparable to that obtained using the true generating kernel, direct inference via PFN, DKL and RFF.

Table 1 reports GP regression accuracy and inference time on the Kernel Cookbook benchmark. As expected under the Single-Realization Limit, the decoded kernels do not match the Oracle GP, which has access to the true generating kernel. Table 1 further shows that this decoder achieves predictive performance close to that of the PFN itself, while consistently outperforming optimization-based methods such as DKL and RFF on more complex kernel families. This behavior is expected in the limited-context regime: *with only a small number of observations, iterative kernel learning methods struggle to reliably optimize high-dimensional kernel parameterizations, whereas the PFN and the decoder leverage amortized inference learned from a broad prior distribution*. As a result, the decoded kernels retain much of the predictive power of the PFN while avoiding the brittleness of test-time optimization. Importantly, this accuracy is achieved with substantial computational savings: kernel construction via the decoder requires a single forward pass ($\sim 10^{-3}$ seconds), compared to several seconds for DKL and RFF, yielding speedups of approximately three orders of magnitude. Pictorial representation of K_{pred} ’s of single-realization setting is given in Figure 13 of Appendix D.

A key practical advantage of our amortized framework is

Table 1. Accuracy and efficiency on the Kernel Cookbook. We compare MSE and inference time (seconds) using 100 context points. We consider Oracle is the true generating kernel. The Single-Realization Decoder achieves comparable accuracy to iterative baselines (DKL, RFF) while producing kernels in a single forward pass, yielding orders-of-magnitude reductions in inference time.

True Kernel	Oracle	Decoder (Ours)		PFN		DKL		RFF	
	MSE	MSE	Time (s)						
RBF	2.89×10^{-5}	2.52×10^{-3}	0.004	6.56×10^{-5}	0.002	2.52×10^{-4}	2.08	4.33×10^{-3}	1.49
Periodic	1.99×10^{-3}	2.78×10^{-2}	0.005	1.01×10^{-2}	0.002	3.80×10^{-2}	2.17	5.51×10^{-2}	1.43
RBF + Periodic	9.12×10^{-3}	1.80×10^{-2}	0.005	7.31×10^{-3}	0.002	1.76×10^{-2}	2.09	3.78×10^{-2}	1.49
RBF \times Periodic	3.50×10^{-3}	2.11×10^{-2}	0.006	8.71×10^{-3}	0.002	2.79×10^{-2}	2.06	4.58×10^{-2}	1.48
SM ($Q = 1$)	7.90×10^{-5}	1.04×10^{-3}	0.004	2.25×10^{-4}	0.002	5.05×10^{-2}	2.14	9.76×10^{-2}	1.47
SM ($Q = 2$)	2.66×10^{-5}	5.73×10^{-4}	0.004	2.30×10^{-4}	0.003	2.87×10^{-2}	2.09	6.51×10^{-2}	1.44
SM ($Q = 4$)	1.47×10^{-5}	2.54×10^{-3}	0.005	2.46×10^{-4}	0.002	2.70×10^{-2}	2.14	5.72×10^{-2}	1.64

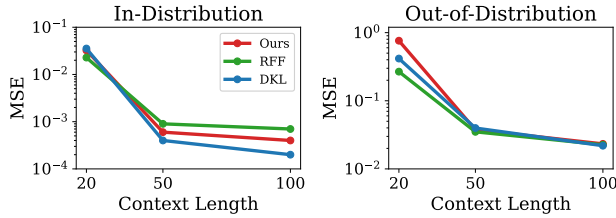


Figure 5. Comparison of MSE (Log scale) on in-distribution (left) and out-of-distribution (right) tasks. In both the cases our framework gives comparable MSE to DKL and RFF baselines. As DKL and RFF require iterative optimization (approximately 1.44–2.17 seconds per task), our decoder produces a kernel in under 10^{-3} seconds via a single forward pass leading to $\approx 1000\times$ reduction in inference time. Out-of-Distribution data is non-Gaussian triangle waves with random frequencies $\sim U(1.0, 3.0)$.

inference efficiency in terms of speed and varying context. Figure 5 compares GP regression MSE obtained using kernels constructed by our Single-Realization Decoder against DKL and RFF for different context length i.e data points in function realization. Across both in-distribution and out-of-distribution benchmarks, the decoded kernels achieve predictive performance on the same scale as these iterative baselines, despite requiring no test-time optimization.

6.3. Scaling Multi-Realization Decoder

We evaluate the scalability of the *multi-realization* decoder to higher input dimensions, using the same decoder and inference procedure as before, with $M = 16$ function realizations sampled from a shared GP prior. The PFNs are also trained on additive GP data in higher dimensions. To avoid requirement of very large context size due to *curse of dimensionality*, each function is generated using an additive kernel with a small number of active dimensions, ensuring well-conditioned covariance structure. We use $N = 500$ for context. Full data generation and training details are provided in Appendix F.

We evaluate scaling using the Kernel cookbook experiment: the decoder receives 16 realizations from a shared kernel, reconstructs a kernel analytically from predicted spectral parameters, and is evaluated via GP regression on held-out

Table 2. Scaling behavior of the multi-realization decoder using 16 function realizations. Periodic kernels remain challenging due to global structural constraints.

Kernel (Additive)	Oracle GP MSE	Amortized MSE
RBF (5D)	1.3×10^{-4}	2.9×10^{-4}
SM ($Q=1$, 5D)	1.1×10^{-4}	3.0×10^{-4}
SM ($Q=2$, 5D)	1.2×10^{-4}	2.4×10^{-4}
SM ($Q=4$, 5D)	1.3×10^{-4}	2.9×10^{-4}
Periodic (5D)	2.6×10^{-4}	9.5×10^{-3}
RBF (10D)	1.30×10^{-4}	3.25×10^{-4}
SM ($Q=1$, 10D)	1.15×10^{-4}	4.01×10^{-4}
SM ($Q=2$, 10D)	3.19×10^{-4}	5.38×10^{-4}
SM ($Q=4$, 10D)	2.06×10^{-4}	4.56×10^{-4}
Periodic (10D)	2.71×10^{-4}	2.32×10^{-3}

data. Table 2 reports results for additive RBF, periodic, and spectral mixture kernels across 5 and 10 dimensions. It shows that proposed PFN based decoder achieve same order of magnitude MSE error as GP oracle, except periodic kernel having difference of one order of magnitude. Although PFNs do not encode per-dimension identity explicitly, accurate kernel reconstruction remains possible. This is because kernel prediction depends on recovering the *aggregate operator structure* rather than independent per-dimension spectral densities. As a result, predictive performance remains within a small constant factor of optimized GP oracles.

7. Conclusions

We presented an interpretability-driven framework for amortized spectral and kernel discovery from Prior-Data Fitted Networks. We show that PFN attention mechanisms encode decodable spectral structure that can be converted into explicit covariance kernels, enabling fast, zero-shot kernel construction without test-time optimization. While effective, this approach inherits a key limitation of in-context learners: performance degrades as the amount and dimensionality of context data grow, constraining scalability in data-rich regimes (Müller et al., 2025). Further, standard PFNs do not encode dimensionality information of input, thus limiting the capacity to decode per-dimensional structure in higher

dimensions. Future work includes incorporating the decoded spectral representations into downstream tasks such as surrogate-based optimization, control, and scientific modeling, as well as exploring hybrid architectures that combine amortized spectral inference with adaptive context selection to improve scalability.

References

Adriaensen, S., Rakotoarison, H., Müller, S., and Hutter, F. Efficient bayesian learning curve extrapolation using prior-data fitted networks. In *Advances in Neural Information Processing Systems 37*. NeurIPS, 2023.

Chang, P. E., Loka, N., Huang, D., Remes, U., Kaski, S., and Acerbi, L. Amortized probabilistic conditioning for optimization, simulation and inference, 2025. URL <https://arxiv.org/abs/2410.15320>.

Cordonnier, J.-B., Loukas, A., and Jaggi, M. On the relationship between self-attention and convolutional layers. In *International Conference on Learning Representations*, 2020.

Duvenaud, D., Lloyd, J. R., Grosse, R., Tenenbaum, J. B., and Ghahramani, Z. Structure discovery in nonparametric regression through compositional kernel search, 2013. URL <https://arxiv.org/abs/1302.4922>.

Garnelo, M., Rosenbaum, D., Maddison, C. J., Ramalho, T., Saxton, D., Shanahan, M., Teh, Y. W., Rezende, D. J., and Eslami, S. M. A. Conditional neural processes, 2018. URL <https://arxiv.org/abs/1807.01613>.

Jenson, D., Navott, J., Zhang, M., Sharma, M., Semenova, E., and Flaxman, S. Transformer neural processes - kernel regression, 2025. URL <https://arxiv.org/abs/2411.12502>.

Lee, J., Lee, Y., Kim, J., Kosiorek, A., Choi, S., and Teh, Y. W. Set transformer: A framework for attention-based permutation-invariant neural networks. In *International Conference on Machine Learning (ICML)*, pp. 3744–3753, 2019.

Lloyd, J. R., Duvenaud, D., Grosse, R., Tenenbaum, J. B., and Ghahramani, Z. Automatic construction and natural-language description of nonparametric regression models, 2014. URL <https://arxiv.org/abs/1402.4304>.

Müller, S. et al. Position: The future of bayesian prediction is prior-fitted. In *Forty-second International Conference on Machine Learning Position Paper Track*, 2025.

Müller, S., Hollmann, N., Arango, S. P., Grabocka, J., and Hutter, F. Transformers can do bayesian inference, 2024. URL <https://arxiv.org/abs/2112.10510>.

Nadaraya, E. A. On estimating regression. *Theory of Probability & Its Applications*, 9(1):141–142, 1964.

Nagler, T. Statistical foundations of prior-data fitted networks. In *Proceedings of the 40th International Conference on Machine Learning*, volume 202 of *Proceedings of Machine Learning Research*, pp. 25660–25676. PMLR, jul 2023.

Ober, S. W., Rasmussen, C. E., and van der Wilk, M. The promises and pitfalls of deep kernel learning, 2021. URL <https://arxiv.org/abs/2102.12108>.

Rahimi, A. and Recht, B. Random features for large-scale kernel machines. In Platt, J., Koller, D., Singer, Y., and Roweis, S. (eds.), *Advances in Neural Information Processing Systems*, volume 20, 2007.

Rasmussen, C. E. and Williams, C. K. I. *Gaussian Processes for Machine Learning*. MIT Press, Cambridge, MA, 2006.

Sharma, K., Singh, S., and Pareek, P. Decoupled-value attention for prior-data fitted networks: Gp inference for physical equations, 2025. URL <https://arxiv.org/abs/2509.20950>.

Sitzmann, V., Martel, J. N. P., Bergman, A. W., Lindell, D. B., and Wetzstein, G. Implicit neural representations with periodic activation functions, 2020. URL <https://arxiv.org/abs/2006.09661>.

Stein, M. L. *Interpolation of spatial data*. Springer Series in Statistics. Springer-Verlag, New York, 1999. ISBN 0-387-98629-4. doi: 10.1007/978-1-4612-1494-6. URL <http://dx.doi.org/10.1007/978-1-4612-1494-6>. Some theory for Kriging.

Tancik, M., Srinivasan, P. P., Mildenhall, B., Fridovich-Keil, S., Raghavan, N., Singhal, U., Ramamoorthi, R., Barron, J. T., and Ng, R. Fourier features let networks learn high frequency functions in low dimensional domains, 2020. URL <https://arxiv.org/abs/2006.10739>.

Tsai, Y.-H. H., Bai, S., Yamada, M., et al. Transformer dissection: A unified understanding of Transformer’s attention via the lens of kernel. In *Proceedings of the 2019 Conference on Empirical Methods in Natural Language Processing and the 9th International Joint Conference on Natural Language Processing (EMNLP-IJCNLP)*, pp. 4344–4353, 2019.

Wilson, A. G., Hu, Z., Salakhutdinov, R., and Xing, E. P. Deep kernel learning, 2015. URL <https://arxiv.org/abs/1511.02222>.

A. Interpretability Experiments: Experimental Protocols

A.1. Data Generation

For all experiments, we generate sinusoidal signals on $x \in [-1, 1]$ with 200 points. Frequencies are sampled uniformly from $[0.5, 5.0]$ Hz with random phases $\phi \sim \mathcal{U}[0, 2\pi]$. For weighted signals,

$$y = a \cdot \sin(2\pi f_1 x + \phi_1) + (1 - a) \cdot \sin(2\pi f_2 x + \phi_2)$$

A.2. PFN Preprocessing

Following the PFN training protocol, we normalize inputs as:

$$Y_{\text{norm}} = \frac{Y - \mu}{\sigma}, \quad \text{then apply sigmoid activation: } Y_{\text{proc}} = \sigma(0.75 \cdot Y_{\text{norm}}).$$

A.3. Representation Extraction

We extract four representations from the PFN:

- $K = x_{\text{enc}}(x)$: Fourier feature encoding of positions
- $V = y_{\text{enc}}(y)$: MLP encoding of values
- $Q = x_{\text{enc}}(x)$: Query encoding (identical to K)
- $H = \text{CrossAttention}(Q, K, V)$: Latent output after 6 transformer layers

For probing, we mean-pool over positions:

$$\bar{H} = \frac{1}{N} \sum_i H[i].$$

A.4. Probing Methodology

We use Ridge regression ($\alpha = 1.0$) for linear probing and 3-layer MLPs ($256 \rightarrow 128 \rightarrow 64$, LayerNorm, GELU, Dropout = 0.1) for nonlinear probing. Training uses AdamW (lr = 10^{-3}), cosine annealing, and early stopping (patience = 50). Train, validation, test split was kept at 65% / 15% / 20%.

B. Additional Mechanistic Results

Table 3. Probing R^2 scores for spectral parameter extraction using **linear probes**. H consistently dominates V across all targets.

Target	H	V	$H + V$
Single Frequency	0.98	0.21	0.99
Dual Frequencies	0.96	0.00	0.96
Full Spectral (f_1, f_2, a_1, a_2)	0.50	0.00	0.50

Table 4. Full Pooling Ablation Results (R^2).

Task	Mean(H)	Mean(V)	Mean(H+V)	Attn(H)	Attn(V)	Attn(H+V)
Easy (1 param)	0.999	0.000	1.000	1.000	0.000	1.000
Medium (2 params)	0.982	0.000	0.983	0.991	0.000	0.991
Hard (4 params)	0.560	0.000	0.564	0.610	0.000	0.602
Very Hard (6 params)	0.333	0.000	0.342	0.404	0.000	0.399

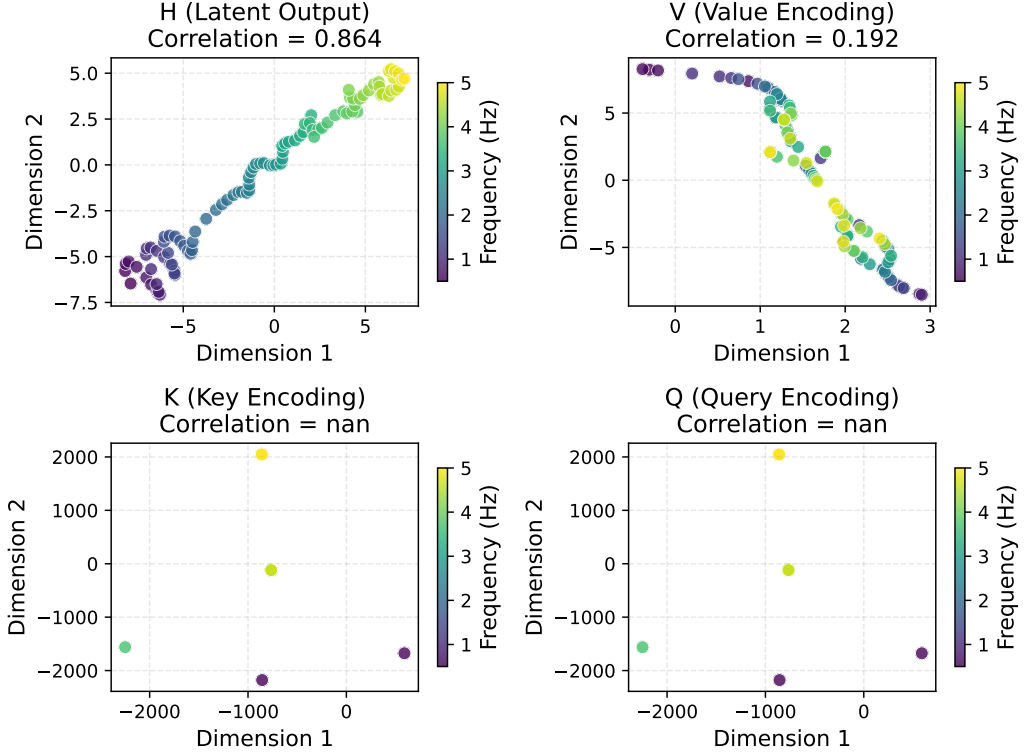


Figure 6. t-SNE visualization of all primary computational stages of PFN representations, with sinusoidal input signals of changing frequency. H shows clear spectral structure ($\rho = 0.86$); V shows partial structure ($\rho = 0.19$); K and Q contain no information about the signal since they come from ϕ_x values due to using decoupled-value attention. Therefore, their t-SNE plots collapse at a few points without any correlation with the input frequency.

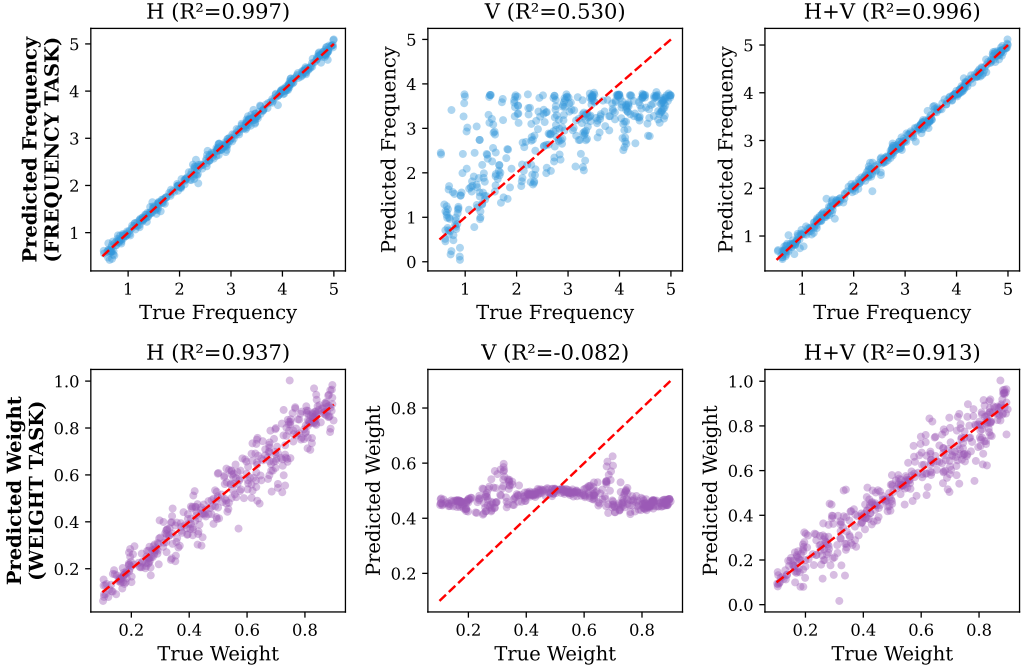


Figure 7. True vs. Predicted scatter for frequency and weight probing (MLP probes). For simple sinusoids with just two components, both frequency and weight regression independently is a fairly simple task, and on H embeddings, a simple MLP is able to achieve 100% accuracy.

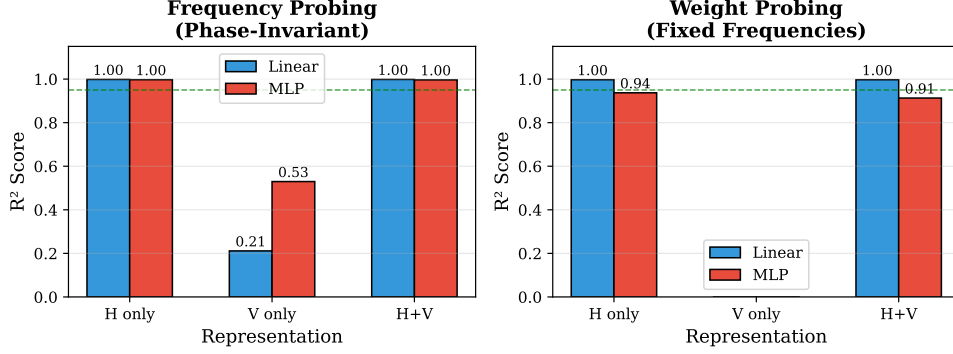


Figure 8. Probing R^2 for frequency (left) and weight (right) prediction, with simple sinusoidal inputs. H+V achieves $R^2 > 0.99$ for both. In frequency probing, MLP achieves much better accuracy than a linear probe in V only representation, suggesting that signal information is present, but in raw form which is later processed through the attention mechanism

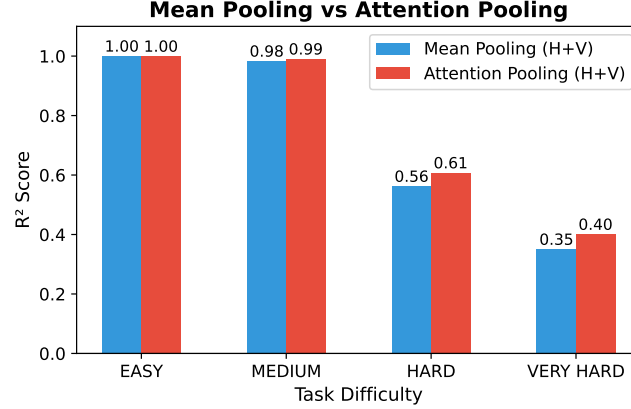


Figure 9. Attention pooling benefit increases with task complexity. This justifies using learned queries in the decoder.

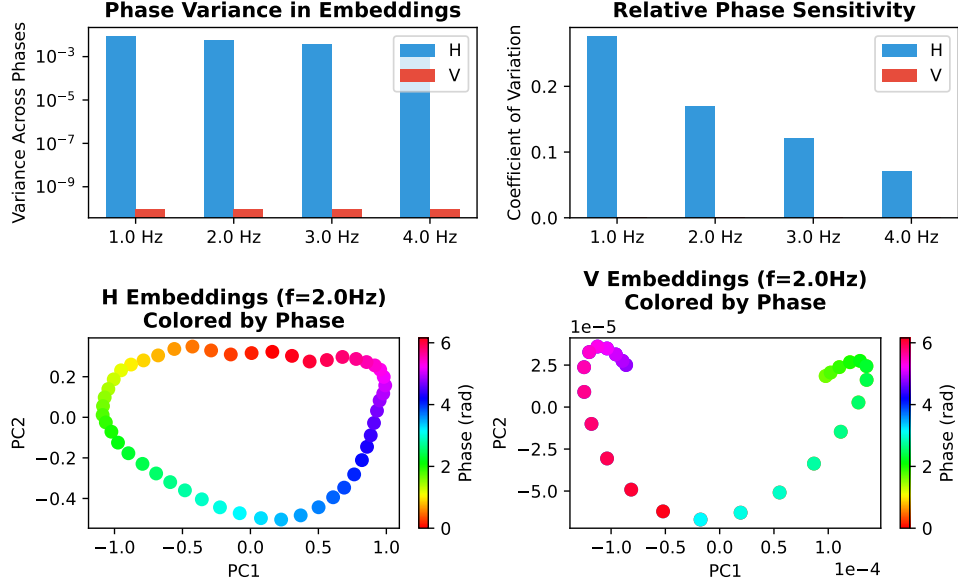


Figure 10. Phase invariance analysis. V embeddings show near-zero variance across phases, while H varies slightly with phase, showing a proper closed circular loop in its PCA plot. This suggests pooling of H and V embeddings rather than using only H for the final decoder task to achieve phase invariance while predicting the spectral density mixture, which doesn't depend on phase of the input.

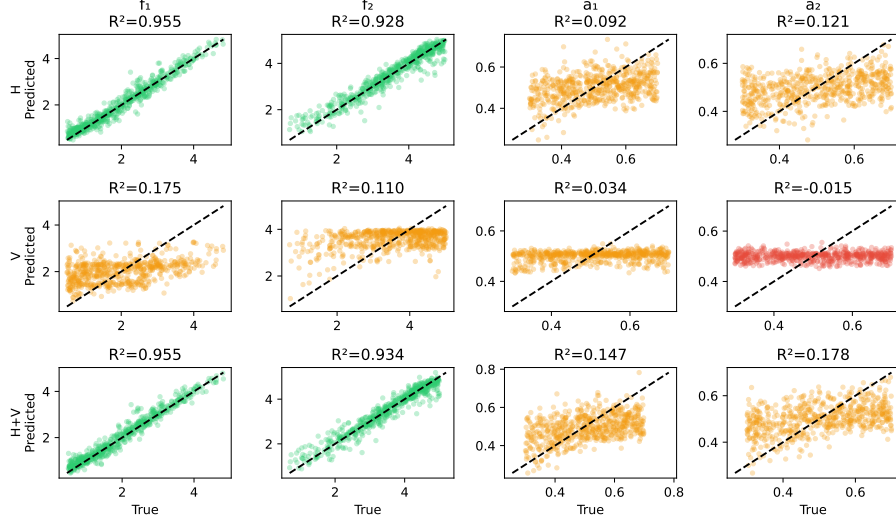


Figure 11. Probing for full spectral parameters (f_1, f_2, a_1, a_2). Frequency prediction succeeds ($R^2 > 0.92$), but amplitude prediction is weak ($R^2 \approx 0.14$). This justifies our decoder architecture of using a filter bank approach for frequency prediction, and a separate network to predict the amplitude. Since amplitude is also discoverable as shown in above experiments, but extracting all the parameters from the weights all at once is difficult for the model.

C. Decoder Details

C.1. Multi-Realization Decoder

The Multi-Realization Decoder estimates the full spectral density from multiple function samples drawn from a common GP prior.

Input. Given $M = 16$ function samples $\{f_m\}_{m=1}^M$ sampled from a GP with unknown spectral mixture kernel, we:

1. Process each sample through the frozen PFN to obtain (H^m, V^m)
2. Aggregate: $\bar{H} = \frac{1}{M} \sum_{m=1}^M H^m$
3. Feed aggregated representations to the decoder

Output: For each active bin b , the decoder predicts (μ_b, σ_b, w_b) where w_b is the relative weight in the spectral mixture.

Kernel Reconstruction: The inferred spectral density is converted to a kernel matrix via Bochner’s theorem. For input locations x, x' with lag $\tau = x - x'$:

$$K(x, x') = \sum_{b: p_b > \eta} w_b \exp(-2\pi^2 \sigma_b^2 \tau^2) \cos(2\pi \mu_b \tau) \quad (5)$$

where $\eta = 0.5$ is the activation threshold.

Data Generation: Training data consists of:

- Spectral parameters: $\mu_q \sim \text{Uniform}[\mu_{\min}, \mu_{\max}], \sigma_q \sim \text{Uniform}[\sigma_{\min}, \sigma_{\max}], w_q \sim \text{Gamma}(2, 1)$
- Kernel: $K = \sum_q w_q \exp(-2\pi^2 \sigma_q^2 \tau^2) \cos(2\pi \mu_q \tau)$
- GP samples: $y^{(m)} \sim \mathcal{N}(0, K), m = 1, \dots, M$

C.2. Single-Realization Decoder

The Single Realization Decoder estimates the kernel structure from a *single* function observation, enabling amortized kernel inference at test time.

As shown in Theorem 4.1, from a single function sample, we can identify *which* frequency components are present, but cannot determine their *relative weights*. Thus, we predict only (μ_b, σ_b) per bin, using equal weights. Analytical scaling is applied as per Theorem 4.2.

Data Generation: Training uses Random Fourier Feature (RFF) signals:

$$y(x) = \sqrt{\frac{2}{n_{\text{rff}} \cdot n_p}} \sum_{q=1}^{n_p} \sum_{j=1}^{n_{\text{rff}}} \cos(2\pi\omega_{qj}x + \phi_{qj}) \quad (6)$$

Here n_p is the number of spectral peaks and $n_{\text{rff}} = 100$ is the number of RFF features sampled per peak. We draw $\omega_{qj} \sim \mathcal{N}(\mu_q, \sigma_q^2)$ and $\phi_{qj} \sim \text{Uniform}[0, 2\pi]$. RFF signals provide cleaner spectral structure than raw GP samples, enabling the decoder to learn peak detection without noise confounds.

C.3. Training Hyperparameters

Table 5 summarizes the training hyperparameters used for the Multi-Realization Decoder and Single Realization Decoder.

Table 5. Training hyperparameters for the Decoders.

Parameter	Multi-Realization Decoder	Single Realization Decoder
n_{samples}	100,000	300,000
n_{points}	200	200
n_{bins}	50	50
d_{model}	128	128
d_{ff}	256	256
n_{queries}	4	4
dropout	0.1	0.1
pos_weight (BCE)	30.0	30.0
λ_{reg}	5.0	5.0
learning rate	1×10^{-3}	1×10^{-3}
weight decay	1×10^{-4}	1×10^{-4}
GP samples (K)	16	1
Frequency range	[0.5, 3.0] Hz	[0.5, 3.0] Hz
Sigma range	[0.01, 0.05]	[0.01, 0.05]
Epochs (Phase 1)	1000	200
Epochs (Phase 2)	1000	200
Epochs (Phase 3)	2000	400

C.4. Architecture Details

Multi-Query Attention Pooler. Given an input sequence H or $V \in \mathbb{R}^{B \times N \times d}$, the model applies a multi-query attention pooling mechanism with learned queries

$$Q \in \mathbb{R}^{1 \times n_q \times d}.$$

The pooled representation is computed as $\text{Linear}(\text{Flatten}(\text{MultiheadAttention}(Q, H, H))) \in \mathbb{R}^{B \times d}$.

Filter Bank Decoder. The decoder operates on two feature sequences $H, V \in \mathbb{R}^{B \times N \times d}$:

$$z_h = \text{MQA}_h(H) \in \mathbb{R}^{B \times d}, \quad z_v = \text{MQA}_v(V) \in \mathbb{R}^{B \times d}.$$

The pooled representations are concatenated and passed through an MLP:

$$z = \text{MLP}([z_h; z_v]) \in \mathbb{R}^{B \times d}.$$

The decoder branches into two prediction heads:

- **Bin classifier:** $\text{Linear}(d, B) \rightarrow p \in \mathbb{R}^B$
- **Parameter head:** $\text{Linear}(d, B \times k) \rightarrow \theta \in \mathbb{R}^{B \times k}$

The parameter dimensionality is: $k = 2$ (Single Realization Decoder: δ, σ) $k = 3$ (Multi-Realization Decoder: δ, σ, w).

C.5. Loss Functions

Binary Cross-Entropy (Bin Classification). The bin classification loss is defined as:

$$\mathcal{L}_{\text{BCE}} = - \sum_b [w_{\text{pos}} \cdot y_b \cdot \log(p_b) + (1 - y_b) \cdot \log(1 - p_b)],$$

where $w_{\text{pos}} = 30$ compensates for sparse positive targets.

Masked Mean Squared Error (Parameter Regression). Parameter regression is applied only to active bins ($y_b = 1$):

$$\begin{aligned} \mathcal{L}_{\text{reg}} = \sum_{b:y_b=1} & \left[(\delta_{\text{pred}} - \delta_{\text{true}})^2 \right. \\ & \left. + 10 (\sigma_{\text{pred}} - \sigma_{\text{true}})^2 + (w_{\text{pred}} - w_{\text{true}})^2 \right]. \end{aligned}$$

C.6. Spectral Mixture Kernel (Bochner's Theorem)

By Bochner's theorem, any stationary kernel can be expressed as the Fourier transform of a spectral density. The spectral mixture model assumes:

$$S(\omega) = \sum_q w_q \cdot \mathcal{N}(\omega \mid \mu_q, \sigma_q^2).$$

The resulting kernel is:

$$\begin{aligned} K(\tau) &= \int S(\omega) e^{2\pi i \omega \tau} d\omega \\ &= \sum_q w_q \exp(-2\pi^2 \sigma_q^2 \tau^2) \cos(2\pi \mu_q \tau). \end{aligned}$$

D. Additional Decoder Results

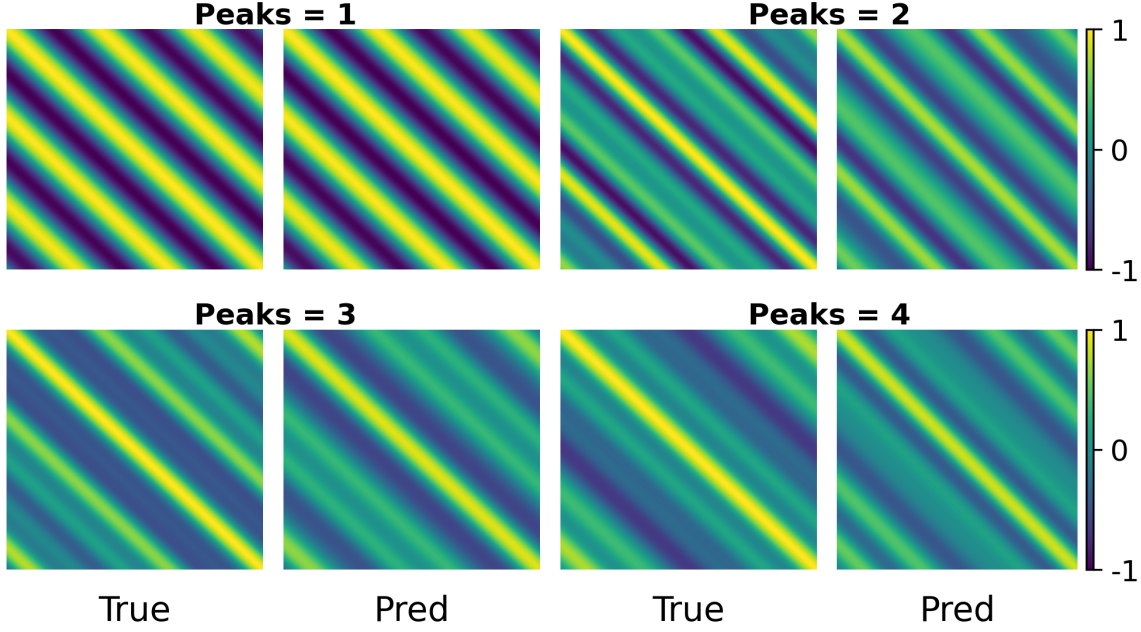


Figure 12. Kernel reconstruction quality using the decoder under **multi-realization settings**. Left: ground truth. Right: decoder prediction. Rows show 1–4 spectral peaks. The decoder accurately captures both periodic structure and spatial correlation patterns across all complexity levels, on seeing 16 sampled functions. The characteristic banded structure induced by periodic components and the diagonal decay associated with finite bandwidth are accurately reproduced, showing that the decoded $S(\omega)$ captures the dominant second-order statistics.

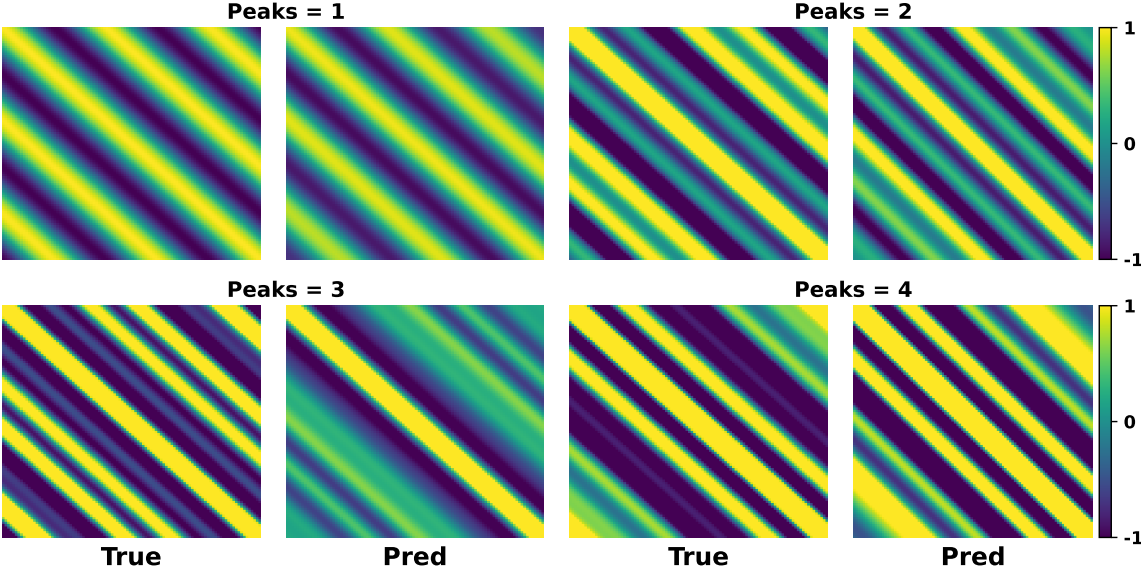
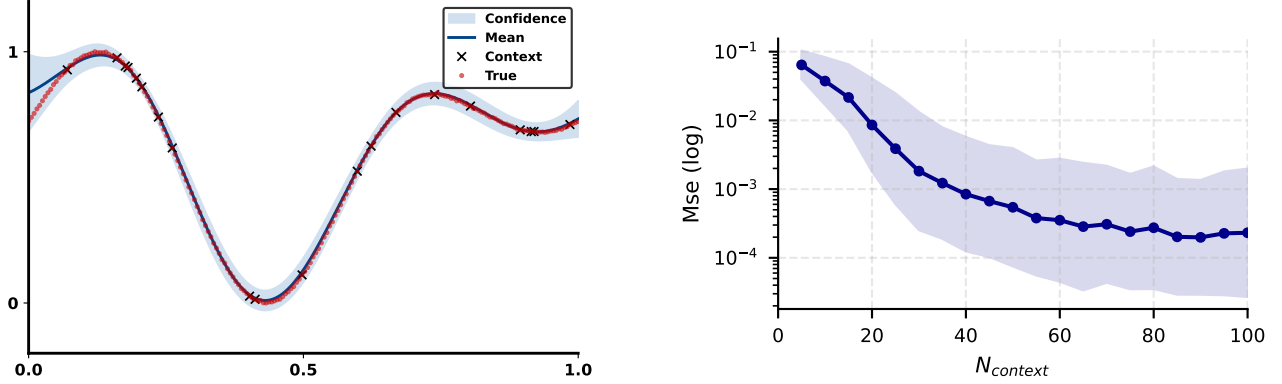


Figure 13. Kernel construction from **single function observations**. Left: ground truth covariance matrices. Right: kernels predicted by the Single-Realization Decoder. While global amplitude is ambiguous, the decoded kernels accurately capture dominant periodic structure and correlation lengthscales.

D.1. GP Performance and Out-of-Distribution Kernels

The Multi-Realization Decoder is trained to recover sparse spectral mixtures, corresponding to stationary kernels with compact frequency support. We therefore evaluate its behavior on kernels that fall outside this assumption, including Matérn



(a) Qualitative GP regression using the kernel recovered by the Single-Realization Decoder with $N = 20$ context observations (black crosses). The predictive mean and $\pm 2\sigma$ confidence intervals are shown.

(b) Mean squared error (MSE) of GP regression using the decoded kernel as a function of the number of context points N_{context} . Shaded regions indicate standard deviation.

Figure 14. Single-Realization Decoder performance.

and squared exponential (RBF) kernels, whose spectral densities are heavy-tailed and require infinitely many mixture components for exact representation.

Table 6 reports results on these out-of-distribution kernels. As expected, performance degrades relative to the oracle GP, which is explicitly parameterized to model these families. Nevertheless, the Multi-Realization Decoder exhibits graceful degradation rather than failure, indicating that PFN representations still encode coarse second-order structure even when the true prior lies outside the model class.

Table 6. Decoder performance measured by MSE on GP regression. Both the oracle GP and our Decoder are conditioned on the same support set of 16 functions drawn from the underlying prior. Kernel parameters are estimated once on the support set and then kept fixed. Reported errors correspond to GP regression performance on 20 unseen test functions drawn from the same prior. RBF and Matérn kernels are out-of-distribution for sparse spectral mixture recovery.

Kernel Family	Oracle GP (MSE)	Ours (MSE)
Periodic	1.33×10^{-4}	1.21×10^{-1}
SM (Q=1)	1.13×10^0	6.15×10^{-4}
SM (Q=2)	1.45×10^{-4}	1.14×10^{-4}
SM (Q=4)	1.17×10^{-4}	2.99×10^{-4}
Out-of-Distribution		
RBF	1.34×10^{-4}	4.76×10^{-3}
Matérn-1/2	9.50×10^{-2}	1.78×10^{-1}
Matérn-3/2	1.14×10^{-1}	2.21×10^{-1}
Matérn-5/2	1.61×10^{-1}	2.94×10^{-1}

Context Scaling for Single-Realization Decoder: Figure 14b reports GP regression MSE as a function of context size. The performance gap between the Single-Realization Decoder and the Oracle remains approximately constant (10–15%) as the number of context points increases from 20 to 200. This behavior is consistent with the theoretical analysis: increasing data improves estimation of the function values but does not resolve the fundamental ambiguity in spectral weights inherent to the single-realization limit.

E. Proofs

E.1. Proof of Theorem 4.1

Proof. Let $\mathbf{f} = (f(x_1), \dots, f(x_N))^\top$ denote the vector of observations. Since $f \sim \mathcal{GP}(0, k)$ is stationary and Gaussian,

$$\mathbf{f} \sim \mathcal{N}(0, K), \quad K_{ij} = k(x_i - x_j).$$

By Bochner's theorem, the kernel admits the spectral representation

$$k(\tau) = \int_{\mathbb{R}} e^{2\pi i \omega \tau} S(\omega) d\omega, \quad S(\omega) = \sum_{q=1}^Q w_q \mathcal{N}(\omega \mid \mu_q, \sigma_q^2).$$

Consider any constant $c > 0$ and define a rescaled spectral density

$$\tilde{S}(\omega) = c S(\omega),$$

with corresponding kernel

$$\tilde{k}(\tau) = c k(\tau).$$

Let $\tilde{f} \sim \mathcal{GP}(0, \tilde{k})$. Then \tilde{f} and f are related in distribution by

$$\tilde{f}(x) \stackrel{d}{=} \sqrt{c} f(x).$$

Let $\tilde{\mathbf{f}} = (\tilde{f}(x_1), \dots, \tilde{f}(x_N))^\top$. Under empirical variance normalization which normalization mirrors the preprocessing used in PFNs, making the model invariant to global rescaling of function values.

$$\hat{\mathbf{f}} = \frac{\mathbf{f} - \bar{f}\mathbf{1}}{\|\mathbf{f} - \bar{f}\mathbf{1}\|_2}, \quad \hat{\tilde{\mathbf{f}}} = \frac{\tilde{\mathbf{f}} - \bar{\tilde{f}}\mathbf{1}}{\|\tilde{\mathbf{f}} - \bar{\tilde{f}}\mathbf{1}\|_2}.$$

Since $\tilde{\mathbf{f}} = \sqrt{c} \mathbf{f}$, it follows immediately that

$$\hat{\tilde{\mathbf{f}}} = \hat{\mathbf{f}}.$$

Therefore, the normalized single-sample distribution induced by the kernel $k(\tau)$ is identical to that induced by $\tilde{k}(\tau) = ck(\tau)$. Because scaling the spectral density corresponds exactly to scaling all weights $\{w_q\}$ by the same constant c , no estimator operating on a single normalized realization can distinguish between $\{w_q\}$ and $\{cw_q\}$.

Consequently, the spectral weights are not identifiable from a single realization, except up to a common multiplicative constant, even as $N \rightarrow \infty$. \square

Remark. Frequency identifiability follows from classical spectral estimation theory: the discrete Fourier transform of a stationary process concentrates energy near the true frequencies, while global rescaling of the covariance affects only the magnitude, not the location, of spectral peaks.

E.2. Proof of Proposition 4.2

Proof. Let $\mathbf{f} = (f(x_1), \dots, f(x_N))^\top \in \mathbb{R}^N$ denote the vector of function values evaluated at the fixed input locations $\{x_i\}_{i=1}^N$. Consider,

$$\mathbf{f} \sim \mathcal{N}(0, \alpha K_{\text{pred}}),$$

where $K_{\text{pred}} \in \mathbb{R}^{N \times N}$ is a fixed positive semi-definite matrix predicated using a single realization decoder and $\alpha > 0$ is an unknown scalar.

We define the squared ℓ_2 norm of \mathbf{f} as $\|\mathbf{f}\|_2^2 = \mathbf{f}^\top \mathbf{f}$. All expectations below are taken with respect to the randomness of \mathbf{f} induced by the Gaussian process, i.e. $\mathbb{E}[\cdot] = \mathbb{E}_{\mathbf{f} \sim \mathcal{N}(0, \alpha K_{\text{pred}})}[\cdot]$.

Since \mathbf{f} is zero-mean Gaussian,

$$\mathbb{E}[\mathbf{f}\mathbf{f}^\top] = \alpha K_{\text{pred}}.$$

Taking the trace on both sides yields

$$\mathbb{E}[\|\mathbf{f}\|_2^2] = \mathbb{E}[\text{tr}(\mathbf{f}\mathbf{f}^\top)] = \text{tr}(\mathbb{E}[\mathbf{f}\mathbf{f}^\top]) = \alpha \text{tr}(K_{\text{pred}}).$$

Therefore, for the estimator

$$\hat{\alpha} = \frac{\|\mathbf{f}\|_2^2}{\text{tr}(K_{\text{pred}})},$$

we obtain

$$\mathbb{E}[\hat{\alpha}] = \frac{\mathbb{E}[\|\mathbf{f}\|_2^2]}{\text{tr}(K_{\text{pred}})} = \alpha,$$

which proves that $\hat{\alpha}$ is an unbiased estimator of the kernel scale. \square

E.3. Proof of Theorem 4.3

Proof. We proceed by showing that multiple independent realizations allow consistent estimation of the covariance function, which uniquely determines the spectral weights.

For a zero-mean stationary Gaussian process, the covariance function

$$k(\tau) = \mathbb{E}[f(x) \cdot f(x + \tau)]$$

fully characterizes the process. By Bochner's theorem (Rasmussen & Williams, 2006), the covariance function $k(\tau)$ is in one-to-one correspondence with the spectral density $S(\omega)$. Therefore, identifying $k(\tau)$ is equivalent to identifying $S(\omega) = \sum_{q=1}^Q w_q \mathcal{N}(\omega \mid \mu_q, \sigma_q^2)$ and its parameters $\{w_q, \mu_q, \sigma_q\}$. We thus show that the empirical covariance converges to $k(\tau)$ as the number of realizations M increases.

Fix any pair of input locations (x_i, x_j) and define the empirical covariance estimator across realizations:

$$\hat{k}_M(x_i, x_j) \triangleq \frac{1}{M} \sum_{m=1}^M [f_m(x_i) \cdot f_m(x_j)].$$

Since the realizations $\{f_m\}$ are independent and identically distributed, each term $f_m(x_i) \cdot f_m(x_j)$ is an independent sample of a random variable with expectation

$$\mathbb{E}[f_m(x_i) \cdot f_m(x_j)] = k(x_i - x_j),$$

where the expectation is taken with respect to the Gaussian process prior.

Moreover, because $f_m(x_i) \cdot f_m(x_j)$ has finite second moment under the Gaussian process prior (Rasmussen & Williams, 2006), the Law of Large Numbers implies

$$\hat{k}_M(x_i, x_j) \xrightarrow{P} k(x_i - x_j) \quad \text{as } M \rightarrow \infty.$$

Since the input grid $\{x_i\}_{i=1}^N$ is fixed and finite, this convergence holds jointly for all pairs (i, j) . Consequently, the entire empirical covariance matrix converges in probability to the true covariance matrix:

$$[\hat{k}_M(x_i, x_j)]_{i,j=1}^N \xrightarrow{P} [k(x_i - x_j)]_{i,j=1}^N.$$

Finally, the limiting covariance function $k(\tau)$ uniquely determines the spectral density $S(\omega)$ via Bochner's theorem. In particular, for the spectral mixture form

$$S(\omega) = \sum_{q=1}^Q w_q \mathcal{N}(\omega \mid \mu_q, \sigma_q^2),$$

the parameters $\{w_q\}$ are uniquely determined by $k(\tau)$. Therefore, as the number of independent realizations M increases, the spectral weights $\{w_q\}$ become identifiable from the empirical second-order statistics of the observed functions. \square

F. High-Dimensional Scaling Details

F.1. Additive Kernel Data Generation in 5D and 10D

Functions are generated from additive Gaussian process priors of the form

$$K(x, x') = \frac{1}{|\mathcal{D}|} \sum_{d \in \mathcal{D}} K_d(x_d, x'_d),$$

where \mathcal{D} denotes the set of active dimensions and each K_d is a one-dimensional kernel (RBF, periodic, or spectral mixture).

To reduce geometric complexity in high dimensions and isolate kernel structure, input locations are generated independently per dimension and sorted along each coordinate. Concretely, for each dimension d , inputs $x_d \in [0, 1]$ are sampled uniformly and sorted before kernel evaluation. This removes combinatorial spatial variation while preserving the temporal or functional structure induced by each kernel.

Only a small subset of dimensions is active for any given function (between 2 and 4 in 5D, and following a curriculum in 10D), ensuring well-conditioned covariance matrices. Product kernels are deliberately avoided, as multiplicative composition across dimensions leads to rapid covariance collapse and destroys additive structure in higher dimensions.

F.2. PFN Training in Higher Dimensions

PFNs in 5D and 10D use the same architecture and hyperparameters as in the one-dimensional setting. The only modification is the use of additive kernels during data generation. Eigenvalue decay analysis confirms that the resulting kernels remain low-rank and structurally well-conditioned.

F.3. Decoder Training and Curriculum in 10D

While the decoder architecture is unchanged across dimensions, training in 10D employs a curriculum to mitigate increased combinatorial ambiguity. Training proceeds in four phases: (1) two active dimensions, (2) three active dimensions, (3) four active dimensions, and (4) up to six active dimensions. This curriculum stabilizes learning without introducing dimension-specific supervision.

F.4. Kernel Cookbook Evaluation Protocol

For each task, 16 functions are sampled from a shared kernel and provided to the decoder. The decoder predicts spectral parameters and reconstructs a kernel analytically using Bochner’s theorem. This kernel is then used for Gaussian process regression on held-out data and compared against a fully optimized GP oracle.

F.5. PFN Encoder Definitions

The spatial encoder $\phi_x(x)$ is implemented as a learnable Fourier Feature mapping. It projects scalar inputs $x \in \mathbb{R}$ onto a fixed bank of frequencies $\mathbf{b} \in \mathbb{R}^{d/2}$, sampled from $\mathcal{N}(0, \sigma^2)$ at initialization. These projections are passed through sinusoidal activations and a learnable linear mixing layer $W \in \mathbb{R}^{d \times d}$:

$$\phi_x(x) = W [\sin(2\pi\mathbf{b}x) \parallel \cos(2\pi\mathbf{b}x)], \quad (7)$$

where \parallel denotes concatenation. The value encoder $\phi_y(y)$ is defined as a three-layer Multi-Layer Perceptron (MLP) with GELU activations, mapping scalar targets y to the latent dimension d .